

Air temperature perturbation in La Malinche volcano area, Tlaxcala, Mexican Highland

Hipólito Muñoz-Nava¹, Silvia Chamizo-Checa¹, Juan Suárez-Sánchez², Elena M. Otazo-Sánchez³, Sandra García-de-Jesús² and Guillermina Barrientos-Rivera²

Abstract

Evaluating air temperature perturbation is important to know the anthropic activity's effect on the environmental system. The study case was La Malinche volcano, concerning the urban, agricultural, and forest environments. The air temperature data (average, maximum, minimum, standard deviation and range), was analyzed by principal components analysis (PCA), and the Kruskal-Wallis (K-W) test. Data analyses were made on a diurnal (warming and cooling rates), daily and monthly basis. The K-W test showed that warming and cooling rates are significantly different between the agricultural, urban, and forest zones, despite the north and south sides of La Malinche volcano had significant differences. The PCA indicated more perturbation concerning the cooling rates of air temperature among the environments than the warming rates. The average, maximum, and minimum air temperature of the urban environment and the standard deviation and range of the agricultural environment were the highest. The minimum air temperature changes more than the maximum in the volcano's urban, agricultural, and forest south side. The K-W test showed that the environmental conditions differed significantly based on average and maximum. The daily air temperature on the north side of La Malinche Volcano was very different from the south side. The PCA with average, maximum, minimum, standard deviation, and range showed that the environments are modified. The average monthly air temperature in the agricultural and forest areas was lower than average. Minimum air temperature increase was more accentuated in urban areas than in agriculture and forest areas and increased more than maximum.

Key words: cooling and warming rates, principal components, environmental effects, air temperature, disturbance degree.

Resumen

La evaluación de la perturbación de la temperatura del aire es muy importante para conocer el efecto de las actividades antrópicas en el sistema ambiental. El área de estudio fue el ambiente urbano, agrícola y forestal en la zona del volcán La Malinche. Utilizamos cinco estadísticas de datos de temperatura del aire y se examinaron mediante el análisis de componentes principales (PCA) y la prueba de Kruskal Wallis. El trabajo se realizó sobre una base diurna (tasas de calentamiento y enfriamiento), diaria y mensual. La prueba K-W mostró que las tasas de calentamiento y enfriamiento son significativamente diferentes entre las zonas agrícolas, urbanas y forestales, incluso, los lados norte y sur del volcán La Malinche tuvieron diferencias significativas. El PCA indicó que había más perturbación en relación con las tasas de enfriamiento de la temperatura del aire entre los ambientes que con las tasas de calentamiento. La temperatura del aire promedio, máxima y mínima de un ambiente urbano y la desviación estándar y el rango de un ambiente agrícola fueron las más altas. La temperatura mínima del aire cambia más que la máxima del lado sur urbano, agrícola y forestal del volcán. La prueba K-W mostró que las condiciones ambientales eran significativamente diferentes según el promedio y el máximo. La temperatura del aire diaria en el lado norte de la Malinche difirió significativamente de la del lado sur. El PCA con promedio, máximo, mínimo, desviación estándar y rango, mostró que los ambientes se encuentran perturbados. La temperatura media mensual del aire en las zonas agrícolas y forestales fue inferior a lo normal. El aumento de la temperatura mínima del aire fue más acentuado en las zonas urbanas que en las zonas agrícolas y forestales y aumentó más que el máximo.

Palabras clave: tasas de enfriamiento y calentamiento, componentes principales, entorno, temperatura del aire, grado de perturbación

Received: October 13, 2023; Accepted: April 26, 2024; Published on-line: July 1, 2024.

Editorial responsibility: Dr. José Gómez Valdés

* Corresponding author: Silvia Chamizo Checa, silchamiz@gmail.com

¹ Universidad Autónoma de Tlaxcala, Licenciatura en Ciencias Ambientales. Facultad de Agrobiología, Tlaxco-Tlaxcala., México.

² Universidad Autónoma de Tlaxcala, Licenciatura en Biología. Facultad de Agrobiología, Ixtacuitla-Tlaxcala., México.

³ Universidad Autónoma del Estado de Hidalgo, Área Académica de Química, Instituto de Ciencias Básicas e Ingeniería, Pachuca, Hidalgo, México.

Hipólito Muñoz Nava, Silvia Chamizo Checa, Juan Suárez Sánchez, Elena María Otazo Sánchez, Sandra Gracia de Jesús, Guillermina Barrientos Rivera

<https://doi.org/10.22201/igeof.2954436xe.2024.63.3.1750>

1. Introduction

The air temperature is an indicator of the structure, functionality, and geographic location of environmental systems and plays an essential role in biological and ecological functions. Similarly, body temperature is a crude indicator of basal metabolism (Prot-siv *et al.*, 2020). The environmental air temperature depends on latitude (Fuelner *et al.*, 2013) and altitude (Hemond and Fechner, 2015; Isaak *et al.*, 2018; Chen *et al.*, 2018) and is influenced by many factors (Sun, 2016), such as time on day, weather, surface type, geographical location, and elevation. Therefore, the spatial and temporal study of the air temperature and their relationship to the anthropic environment modifications are of great interest as urban areas and land-use change. Furthermore, temperature increase can dramatically affect the cells of living organisms and the populations, with ecological consequences (Waldock *et al.*, 2018), by altering the relationships between biodiversity and the functioning of ecosystems (García *et al.*, 2018), increasing the respiration rate and decreasing the plants' photosynthesis (Duffy *et al.*, 2021).

The effect of environmental modifications on air temperature has been analyzed by comparing rural and urban areas or their surroundings; in places where buildings abound, the temperature is higher than in other areas (Suomi and Käyhkö, 2012; Wiesner *et al.*, 2014; Zhou *et al.*, 2017). Vitt *et al.*, 2015, reported that rural areas show lower average, maximum, and minimum temperatures than urban areas, derived from constructions and reduced vegetation (Shiflett *et al.*, 2017). The change of natural conditions by asphalt and concrete creates the phenomenon called urban heat island due to the vast urbanization in large cities (Zelevánková *et al.*, 2015; Vuckovic *et al.*, 2017). The spatial and temporal heat island and heat wave combination act synergistically (Li and Bou-Zeid, 2013). The difference between urban and rural areas can be naturally due to altitude and latitude; it depends on the observation time, instrumentation, and the location of the measuring station (Peterson, 2003).

Environmental temperature differences are relative. For example, the difference is more significant between urban and wetland areas, followed by a body of water and forest (Ayandale, 2017), due to the surface heat island intensity and the type of landscape being more influenced by seasonal, diurnal and climatic factors (Yang *et al.*, 2017). As air temperature is a dynamic variable, the differences between urban and rural areas also depend on seasons and daytime; even in the diurnal cycle, the warming and cooling rates are asymmetric (Bernhardt *et al.*, 2018). The differences are more pronounced in autumn than spring (Wiesner *et al.*, 2014; Suomi and Käyhkö, 2012). Furthermore, these authors reported that the differences between the daily minimum temperatures are more significant, which are not constant during the day and are more pronounced than at night (Oleson, 2012).

Figure 1a shows parallel lines ($f(x)=mx+b$) of a correlated variables system. Each line is a vector $f_i(x)$ multiplied by a scalar α_i . The sum of vectors multiplied by its respective scalar gives a new vector f multiplied by a respective scalar α , which is to say, the lines are a linear combination. This new vector is the principal component and represents the linear combination of the original variables (Joliffe and Cadima, 2016). The variables of this example can be represented perfectly by the principal component (Figure 1b) due to the correlations or loading between the original variables, and the principal component is equal to 1. Similarly, in an undisturbed environment, the gradual change of air temperature in a topography area can be represented graphically as parallel lines or patterns and then by principal components. On the contrary, when a line is not parallel to the others (Figure 2a) due to the system being modified or perturbed, the variables are represented by two principal components (Figure 2b). In the first example, one principal component represents all original variables; in the second example, the representation is partitioned by two components. The use of principal components to explore patterns and perturbations is reported in the literature (Abid *et al.*, 2018; Blommer and Rehm, 2014; Imtiaz and Sarwate, 2016; Hajrya and Mechbal, 2013). On the basis above described, we analyzed the modifications of air temperature gradient among urban, agricultural, and forest environments in the Mexican Highland.

2. Materials and Methods

2.1 Weather stations

Air temperature data recorded on the following weather stations from 2016 to 2019 were used: Huamantla (Hla), located in an agricultural area; Tlaxcala (Tla), located in the urban area of Tlaxcala City; La Malinche I (LMI), and La Malinche II (LMII), both located on the north and south slopes of the La Malinche stratovolcano forest, respectively (Figure 3). The data were obtained from the Mexican Meteorological Service (Servicio Meteorológico Nacional) (SMN) website (<https://smn.conagua.gob.mx/es/observando-el-tiempo/estaciones-meteorologicas-automaticas-ema-s>). Meteorological variables were collected and monitored at these stations based on the World Meteorological Organization (SE, 2013; Fernández *et al.*, 2015). Regarding altitude and distance among the weather stations, the Tla and Hla have a minor altitude difference (10 m) but the most extensive distance (35.3 km). On the other hand, the Hla and LMI have the most remarkable altitude difference (709 m) but are closer (14.1 km). Table 1 shows more data about the weather stations.

The air temperature perturbation among urban, agricultural

and forest environments was analyzed on a diurnal, daily, and monthly basis.

2.2 Diurnal air temperature analysis

The diurnal analysis was carried out using air temperature data registered every 10 minutes (T_{10}). It considered two diurnal intervals: the first corresponds to the warming phase from 7:30 to 14:30, and the second is the cooling phase from 15:30 to 22:30 hours local time. The warming and cooling rates were calculated for each day in both phases. These intervals were selected because the maximum air temperature peak occurs between 14:30 and 15:30 in the study area. The maximum temperature peak is reached at different day hours (Sun, 2016; Nwofor and Dike, 2010). The warming and cooling rates were estimated using the slope of the linear regression equation. Radons *et al.*

(2019) reported better performance of a linear function than the sinusoidal function in the morning, immediately after twilight, when the temperature changes are more pronounced. The linear regression equation used is (McBean and Rovers, 1998):

$$T'_{10} = \alpha + \beta t_i + \varepsilon_i \tag{1}$$

Where:

T'_{10} = air temperature every 10 minutes

α = the ordinate at the origin

β = warming or cooling rate

t_i = every 10 minutes

ε_i = random error

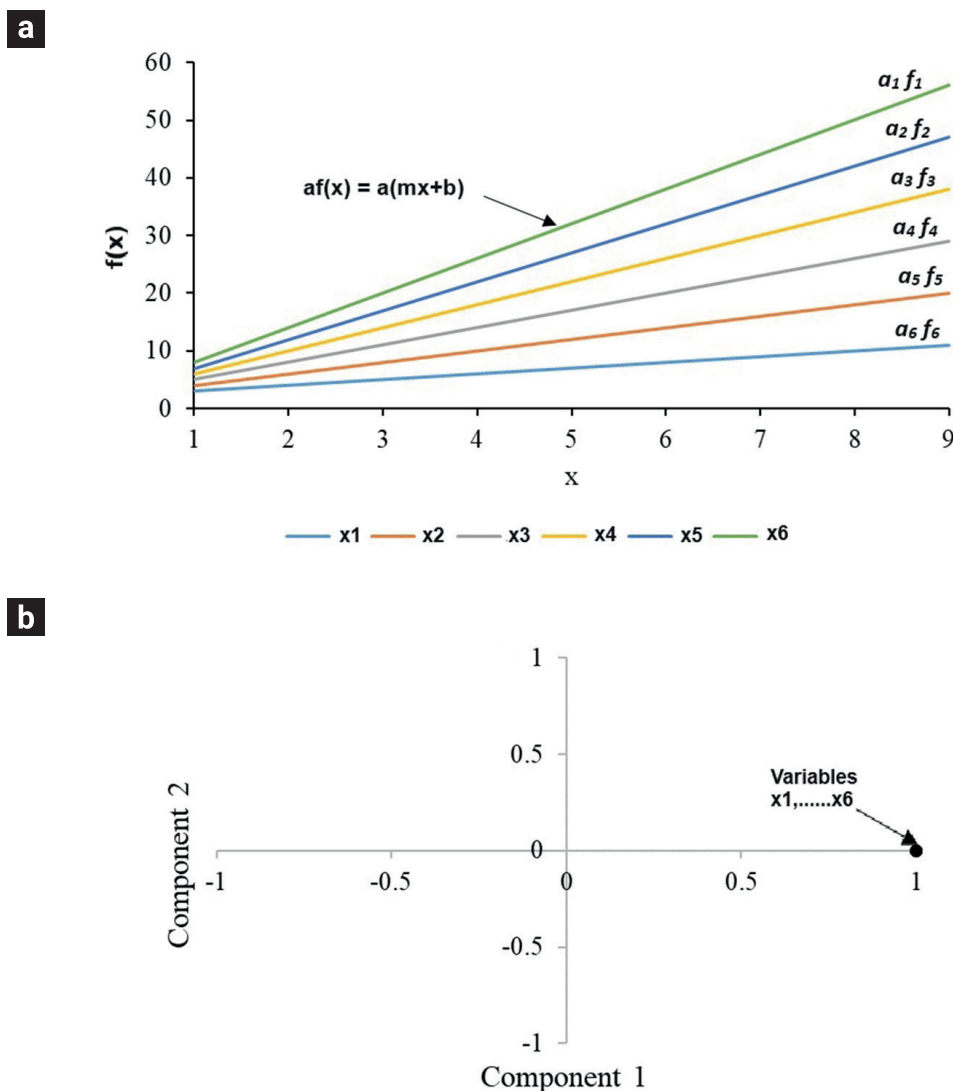


Figure 1. Parallel lines of gradually change variables (a), perfectly represented variables by component 1 (b).

A comparison of warming and cooling rates was made among the four years in a weather station (vertically shaded) and the four weather stations in a year (horizontally shaded) (Table 2). This comparison could be called orthogonal comparison. Ergo resulted in 48 comparisons, for example, *Tla*-16 with *Tla*-17, *Tla*-16 with *Hua*-16, and so on.

The comparison of warming and cooling rates among the years and weather stations was made using the Kruskal-Wallis nonparametric test (McBean and Rovers, 1998):

$$H = \frac{12}{N(N+1)} \left[\frac{R_1^2}{n_1} + \frac{R_2^2}{n_2} + \dots + \frac{R_{16}^2}{n_{16}} \right] - 3(N+1) \quad (2)$$

Where:

H = Kruskal-Wallis statistic

R_1, R_2, \dots, R_{16} = sum of warming or cooling rates in each group

formed by a weather station and a year (a cell in Table 2).

n_1, n_2, \dots, n_{16} = number of warming or cooling rates (observations) in each group (weather station-year)

N = total number of warming or cooling rates in the sixteen groups

The warming and cooling rates were analyzed in the sixteen weather station-year groups using the principal components analysis (PCA). The PCA is a mathematical procedure that transforms a system of correlated variables into another of uncorrelated variables to reduce its dimensionality and determine linear combinations (Daultrey, 1976; Schuenemeyer & Drew, 2011). As in the introduction mentioned, the principal component is the linear combination of original variables and is the new vector multiplied by a scalar or eigenvalue (λ_i), which in turn represents the variance of original variables. In this study, those variables are the warming or cooling rates in the groups. The variables of

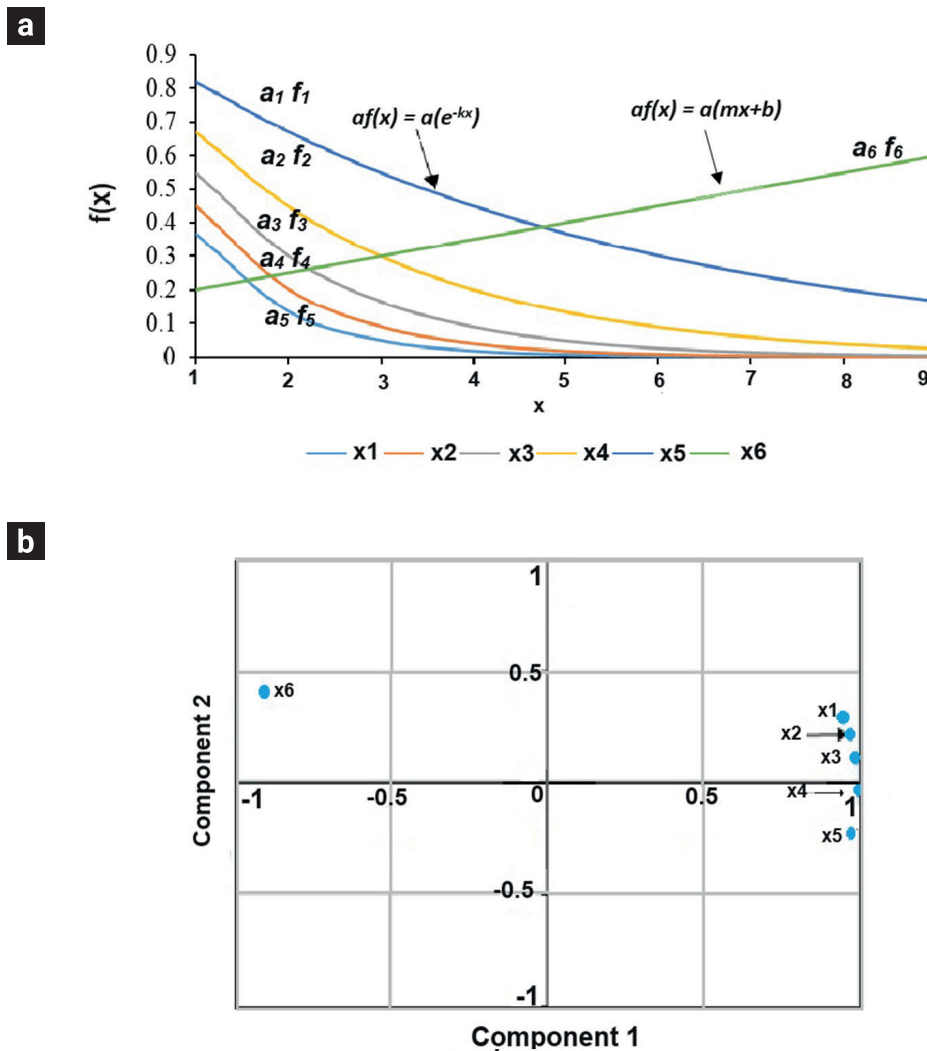


Figure 2. Parallel and no parallel lines of variables (a). Represented variables by two components (b).

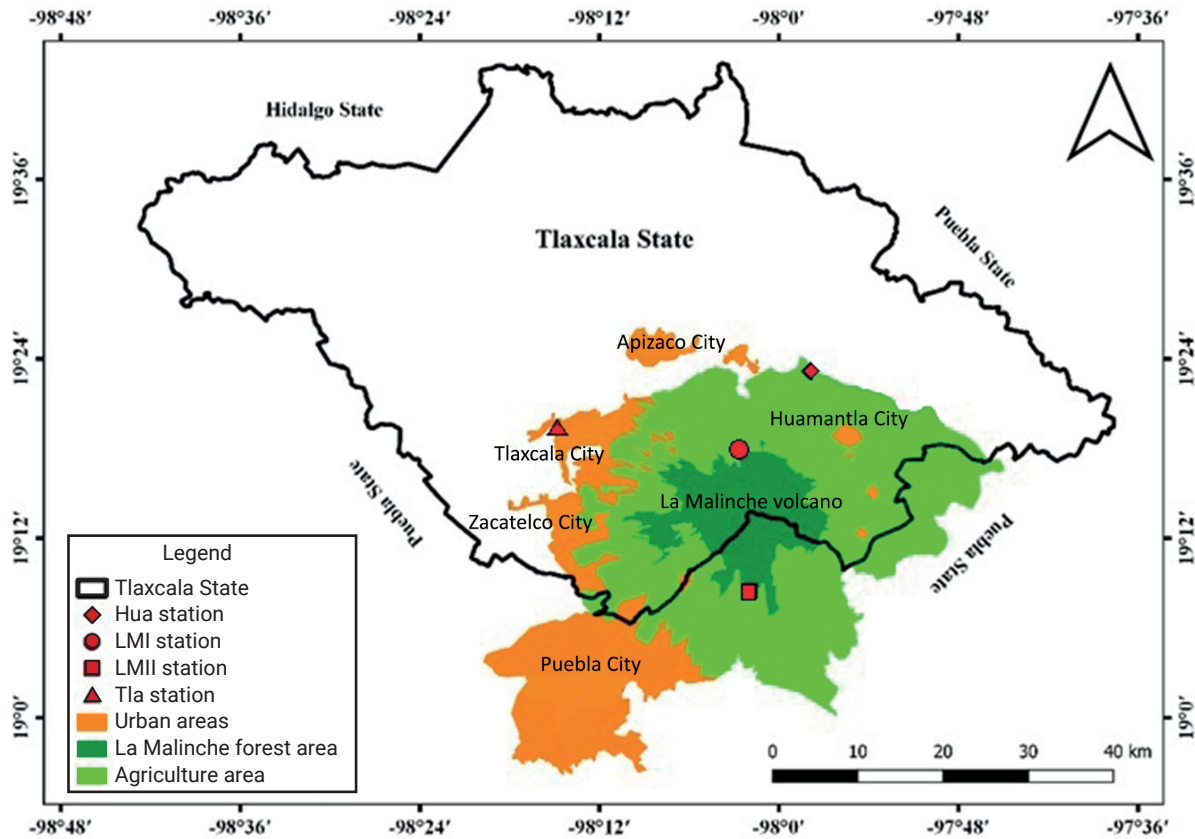


Figure 3. Location of study area.

Table 1. Information on weather stations.

Weather Station	Coordinates		Altitude (*masl)	Type	Environmental condition
	West Latitude	North Longitude			
Tlaxcala (Tla)	98°14'48"	19°19'29"	2232	Synoptic meteorological automatic	Urban (area of Tlaxcala City)
Huamantla (Hla)	97°57'59"	19°23'10"	2222	Meteorological automatic	Agricultural (area of Huamantla Valley)
La Malinche I (LMI)	98°02'39"	19°17'51"	2931	Meteorological automatic	Forest (northern slope of La Malinche volcano)
La Malinche II (LMII)	98°01'56"	19°08'27"	2748	Meteorological automatic	Forest (southern slope of La Malinche volcano)

*masl: meters above sea level

Table 2. Comparison among weather stations and year.

Year	Weather station				
	Tla	Hua	LMI	LMII	##
2016	Tla-16	Hua-16	LMI-16	LMII-16	6
2017	Tla-17	Hua-17	LMI-17	LMII-17	6
2018	Tla-18	Hua-18	LMI-18	LMII-18	6
2019	Tla-19	Hua-19	LMI-19	LMII-19	6
#	6	6	6	6	48

Number of comparisons among the four years in a weather station, ## Number of comparisons among the four weather stations in a year

a system can be represented by one principal component (Figure 1a), and its eigenvalue represents 100% of the variance of the original variables. Otherwise, when the variables are represented by two or more components, the original variables' variance will not be distributed by only one eigenvalue. The eigenvalues were calculated with the characteristic equation of the matrix $\{R\}$:

$$|\{R\} - \lambda_i \{I\}| = 0 \quad (3)$$

Where:

$\{R\}$ = correlation matrix of warming or cooling rates in each group

λ_i = eigenvalues of the principal components

$\{I\}$ = identity matrix

The loads or correlations of the principal components with the warming and cooling rates in each group were calculated with the following matrix equation:

$$\{L\} = \{E\} \cdot \{\Lambda\}^{\frac{1}{2}} \quad (4)$$

Where:

$\{L\}$ = matrix of loads or correlations between the principal components and the warming and cooling rates in each group

$\{E\}$ = matrix of eigenvectors associated with each eigenvalue

$\{\Lambda\}$ = diagonal matrix of λ_i , the elements outside the diagonal are zero

When the original variables are represented by a unique principal component, the loading or correlation of each variable with the principal component is perfected, that is, the element of the first column (l_{1i}) of matrix $\{L\}$ are equal to 1 (Figure 1b); otherwise, all l_{ij} elements are between -1 and 1 (Figure 2b).

2.3 Daily and monthly air temperature analysis

The daily analysis was carried out by grouping the T_{10} data from 00:00 to 23:50 hrs. local time. Therefore, each day had 144 values, with which the daily air temperature statistics: average ($T_{ave,d}$), maximum ($T_{max,d}$), minimum ($T_{min,d}$), standard deviation ($T_{SD,d}$), and range ($T_{Ra,d}$), were estimated for the sixteen weather station-years groups. $T_{max,d}$ and $T_{min,d}$ were selected from the 144 values. $T_{ave,d}$ and $T_{SD,d}$ were calculated using the 144 values. The calculus of $T_{ave,d}$ with the 144 values is more robust because the average is underestimated if it is calculated by $(T_{max,d} + T_{min,d})/2$, due to the assumption of a symmetric rise and fall of temperature during the day (Bernhardt *et al.*, 2018). $T_{Ra,d}$ was calculated subtracting T_{max} from T_{min} . The monthly analysis was carried out by grouping T_{10} data according to the month. The monthly air temperature statistics were similar to daily statistics: average ($T_{ave,m}$), maximum ($T_{max,m}$), minimum ($T_{min,m}$), standard deviation ($T_{SD,m}$) and range ($T_{Ra,m}$). The daily air temperature statistics for the four weather stations and years were analyzed using the K-W test and PCA, just as it was in diurnal air temperature (previous section).

3. Results

3.1 Diurnal air temperature

3.1.1 warming and cooling rates

The correlation coefficients of T_{10} versus time were significant ($p < 0.05$) in all sixteen groups (4 years X 4 weather stations). The box and whisker plots of warming and cooling rates are in Figure 4. The average warming rates had an interval from $2.6 \times 10^{-2} \text{ } ^\circ\text{C} \cdot 10 \text{ min}^{-1}$ (in the *LMI* weather station and 2016 year, abbreviated as *LMI-16*) to $3.4 \times 10^{-2} \text{ } ^\circ\text{C} \cdot 10 \text{ min}^{-1}$ (*Hua-19*). The

minimum warming rate had values from $3.1 \times 10^{-4} \text{ }^\circ\text{C} \cdot 10 \text{ min}^{-1}$ (*LMI-16*) to $6.9 \times 10^{-3} \text{ }^\circ\text{C} \cdot 10 \text{ min}^{-1}$ (*Hua-19*), and maximum warming rates were from $5.0 \times 10^{-2} \text{ }^\circ\text{C} \cdot 10 \text{ min}^{-1}$ (*LMI-16*) to $8.1 \times 10^{-2} \text{ }^\circ\text{C} \cdot 10 \text{ min}^{-1}$ (*Hua-19*). The ranges had values from 5.0×10^{-2} (*LMI-18*) to $7.9 \times 10^{-2} \text{ }^\circ\text{C} \cdot 10 \text{ min}^{-1}$ (*Hua-18*), and the standard deviations were from $9.6 \times 10^{-3} \text{ }^\circ\text{C} \cdot 10 \text{ min}^{-1}$ (*LMI-19*) to $1.5 \times 10^{-2} \text{ }^\circ\text{C} \cdot 10 \text{ min}^{-1}$ (*Hua-17*).

Concerning cooling rates, the average values of the groups were from $-3.0 \times 10^{-2} \text{ }^\circ\text{C} \cdot 10 \text{ min}^{-1}$ (*LMII-17*) to $-2.0 \times 10^{-2} \text{ }^\circ\text{C} \cdot 10 \text{ min}^{-1}$ (*LMI-16*). The minimum cooling rates had values from $-7.4 \times 10^{-2} \text{ }^\circ\text{C} \cdot 10 \text{ min}^{-1}$ (*Hua-16*) to $-3.8 \times 10^{-2} \text{ }^\circ\text{C} \cdot 10 \text{ min}^{-1}$ (*LMI-17*), and the maximum cooling rates were from $-2.2 \times 10^{-3} \text{ }^\circ\text{C} \cdot 10 \text{ min}^{-1}$ (*Hua-19*) to $-1.5 \times 10^{-4} \text{ }^\circ\text{C} \cdot 10 \text{ min}^{-1}$ (*LMI-16*). The cooling rates range were from $3.7 \times 10^{-2} \text{ }^\circ\text{C} \cdot 10 \text{ min}^{-1}$ (*LMI-17*) to $7.4 \times 10^{-2} \text{ }^\circ\text{C} \cdot 10 \text{ min}^{-1}$ (*Hua-16*), and the standard deviation values were from $7.6 \times 10^{-3} \text{ }^\circ\text{C} \cdot 10 \text{ min}^{-1}$ (*LMI-19*) to $1.4 \times 10^{-2} \text{ }^\circ\text{C} \cdot 10 \text{ min}^{-1}$ (*LMII-17*).

3.1.2 Comparing heating and cooling rates

A comparison of the warming and cooling rates groups with K-W is shown in the matrix of Figure 5. The blocks indicate a group (a pair of weather station-years). The black blocks mean that a group had no significant difference ($p > 0.05$), and the grey blocks indicate that a group had a significant difference ($p < 0.05$). The two matrices (Figure 5a and Figure 5b) have similar distribution of the blocks. That means that in the weather station year, the warming and cooling rates are similar with the K-W test, except for the diagonals' blocks marked by the ellipses. The diagonals show that at the *Tla* and *LMI*, and the *LMI* and *LMII* weather stations, the warming rates showed no significant differences, while the cooling rates did. The *Hua* and *LMI* weather stations significantly differed in the warming and cooling rates. The warming and cooling rates in the years in each weather station had no significant difference, except for 2016 and 2017 at the

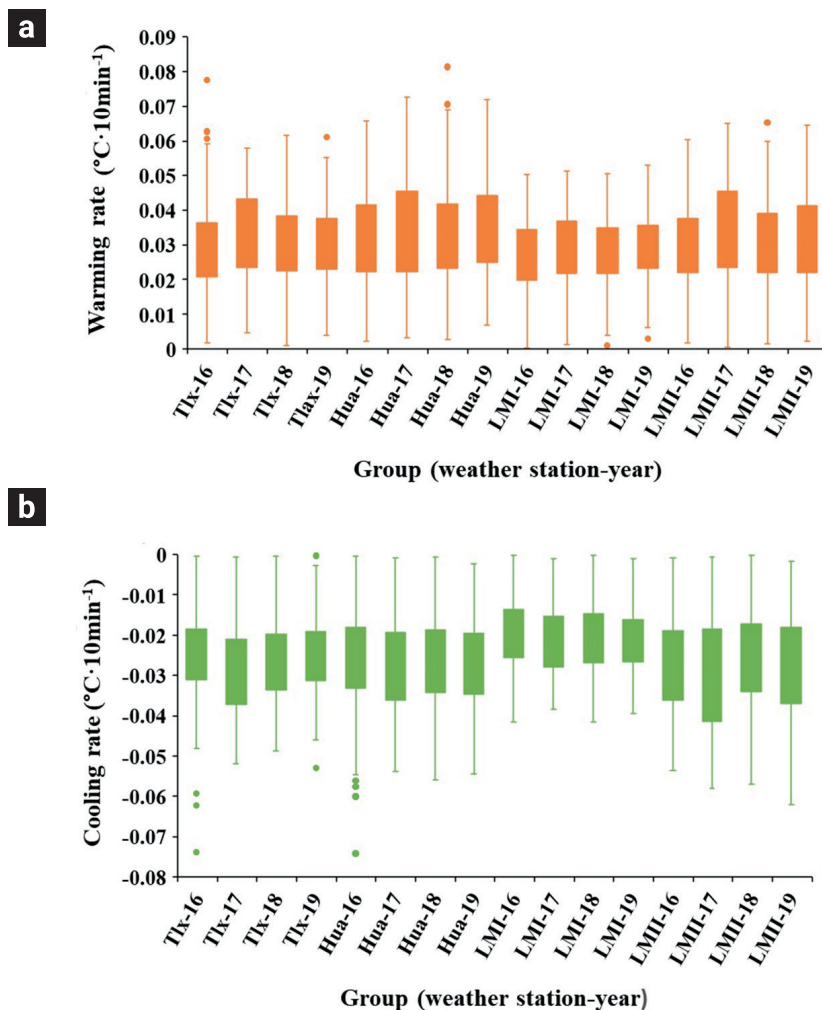


Figure 4. Warming (a) and cooling (b) rates in the groups (weather station-year).

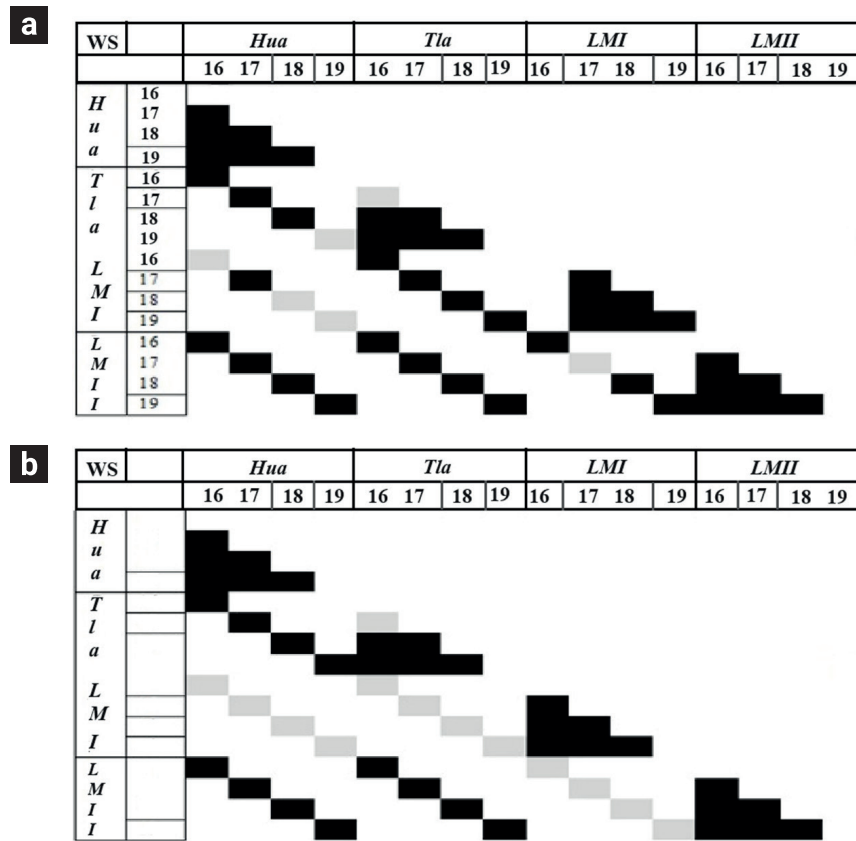


Figure 5. Matrix comparing warming (a) and cooling (b) rates. Black box= no significant difference, grey box= significant difference. WS = Weather station.

Tla weather station. In percentage terms, the matrix warming rates had $(6/48) \cdot 100 = 12.5\%$ of grey blocks, while the matrix cooling rates had $(13/48) \cdot 100 = 27\%$ of grey blocks, both with significant differences.

3.1.3. Principal component analysis of warming and cooling rates

The principal component analysis (PCA) showed that three components represented 84% of the accumulated total variance of warming rates in the sixteen groups (Figure 6). The eigenvalue (λ_i) of each component represents the total variance of the original variable. Components 1, 2, and 3 represented 59%, 18%, and 7% of the total variance, respectively. Figure 7a shows the correlations of the warming rates of the sixteen groups with the components 1 and 2. The correlation or loading between the original variables and components is given by L values (equation 4). The warming rates with component 1 had correlation values from -0.91 to -0.41, and with component 2, they had values from

-0.43 to 0.84 (indicated with red lines in the figures). These correlations values formed two subgroups of weather stations based on years, one composite with 2017, 2018 and 2019, and another with 2016.

Concerning the cooling rates, the PCA showed that 79% of the total variance was represented by three components (Figure 6). Components 1, 2 and 3, correspond to 40, 22 and 17%, respectively. The correlations between cooling rates and the component 1 were from -0.92 to -0.28, and the correlations with the component 2 were from -0.68 to 0.72. Figure 7b shows the correlations of cooling rates with components 1 and 2. It is observed that, unlike the figure of warming rates, the cooling rates form four groups composite by the weather stations according to the years. The groups of cooling rates for 2018 and 2019 have diametrically opposite correlations (positive and negative values) with component 2. The group of cooling rates for 2017 had negative correlations with component 1. The group of cooling rates for 2016 had poorly correlated with component 2.

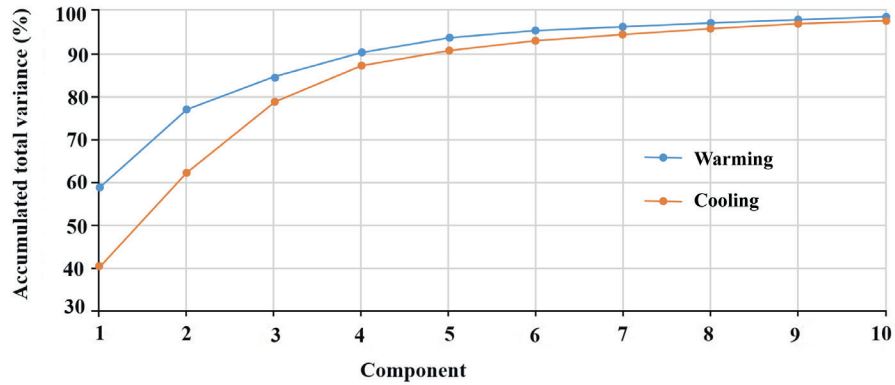


Figure 6. Accumulated total variance of principal components for air temperature warming and cooling rates.

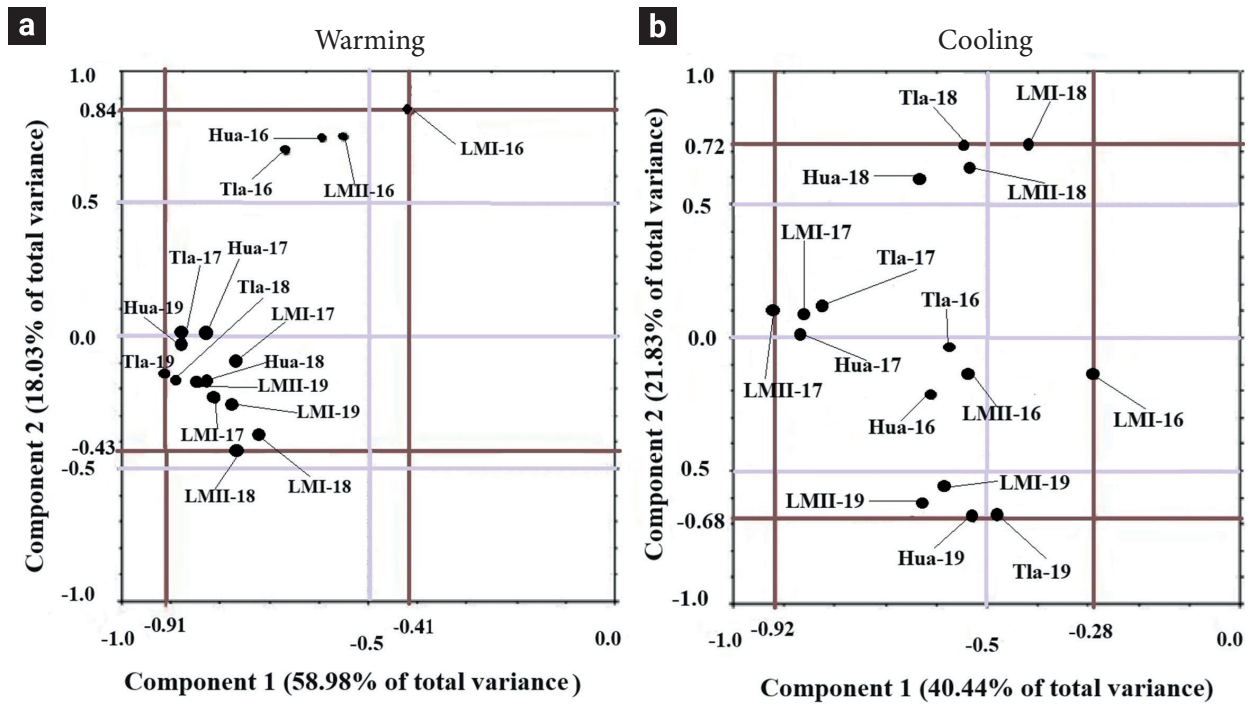


Figure 7. Warming a) and cooling b) rates correlations with two principal components for weather station-year groups.

3.2 Daily air temperature

3.2.1 Average, minimum, maximum, standard deviation, and range

The average ($T_{ave,d}$), minimum ($T_{min,d}$), maximum ($T_{max,d}$), standard deviation ($T_{SD,d}$) and range ($T_{Ra,d}$) daily air temperature, calculated with T_{10} data are depicted in Figure 8. The average daily air temperature (blue line) of the *Tla* weather station is on top, followed by *Hua* (red line), *LMII* (pink line), and *LMI*

(green line) weather stations (Figure 8a), this kind of behavior is shown too in the maximum daily air temperature (Figure 8b), but no like that in the case of minimum air temperature, which behavior was as follows: *Tla*, *LMI*, *LMII*, and *Hua* weather stations (Figure 8b). For the case of standard deviation and range statistics, the *Hua* weather station is on top, followed by *Tla*, *LMII*, and *LMI* weather stations (Figure 8, c, and d). The lowest and highest values and their corresponding date are in Table 3. The lowest $T_{ave,d}$ was calculated in *Hua* weather station, and the highest was calculated in *Tla* weather station. As to $T_{max,d}$, the

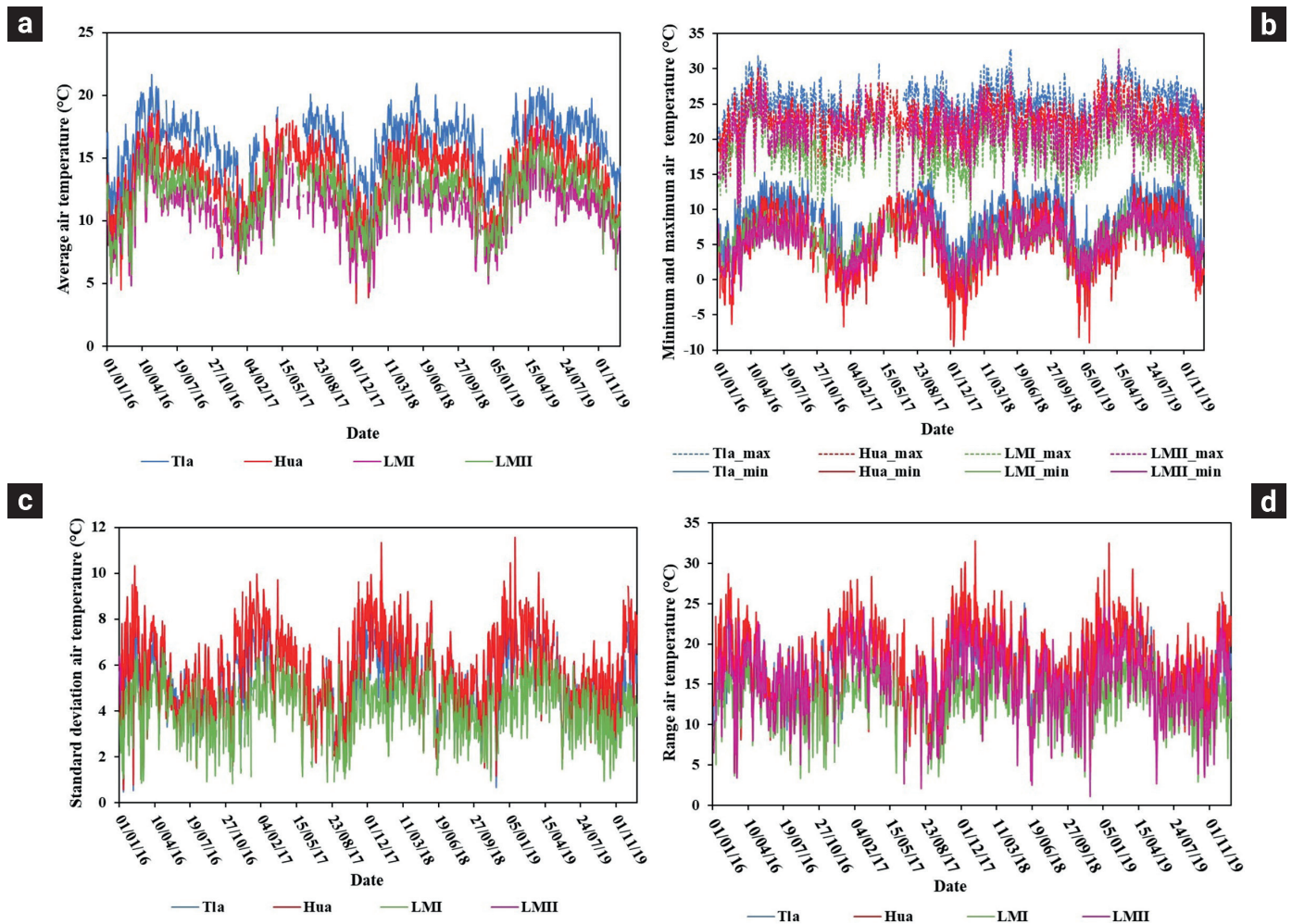


Figure 8. Daily air temperature: a) average, b) minimum and maximum, c) standard deviation, d) range.

Table 3. Lowest and highest values of air temperature statistics.

Statistics	Lowest	Highest
Average daily	Hua-dec-17 Agricultural: 3.4°C	Tla-may-16 Urban: 21.6°C
Maximum daily	LMII-ene-16 South-forest: 6.4°C	LMII-abr-19 South-forest: 32.9°C
Minimum daily	Hua-dec-17 Agricultural: -9.4°C	Tla-oct-17 Urban: 15.4°C
SD daily	LMII-nov-18 South-forest: 0.3°C	Hua-ene-19 Agricultural: 11.5°C
Range daily	LMII-nov-18 South-forest: 1.1 °C	Hua-ene-19 Agricultural: 32.4°C

lowest and highest values were calculated in the *LMII* weather station. The lowest and highest $T_{min,d}$ were calculated in the same weather stations as the calculated for average. Concerning $T_{SD,d}$ and $T_{Ra,d}$, the lowest and highest were calculated in *LMII* and *Hua* weather stations, respectively. The lowest values of these statistics occurred in winter, and the highest occurred in spring.

The most frequent $T_{ave,d}$ and $T_{max,d}$ were higher in the *Tla* weather station from 16 to 18°C and from 25 to 30°C, respectively, than in other weather stations. This weather station recorded 15 days with air temperatures higher than 30°C in 2019. On the other hand, *Hua* weather station registered more days with $T_{min,d}$ below or equal to 0°C than other weather stations. This weather station had 80 days with $T_{min,d}$ below 0°C in 2017, which was a higher number of days than the other three years. The most frequent $T_{SD,d}$ values were from 4 to 6°C in the four weather stations and years. The *Hua* weather station had more days, from 132 to 151, with $T_{SD,d}$ values from 4 to 6°C, except for 2017, in which values from 6 to 7°C in 60 days were calculated. The most frequent $T_{Ra,d}$ values were from 10 to 20°C at the four weather stations. In 2019, the *LMI* weather station had 194 days with $T_{Ra,d}$ values from 10 to 15°C, the highest number of days with this air temperature range.

3.2.2. Comparing daily air temperature statistics

The comparison of daily air temperature statistics of the four weather stations and the four years is presented similarly to the comparison of warming and cooling rates. The matrix comparison of the K-W test for each statistic is in Figure 9. $T_{ave,d}$ and $T_{max,d}$ had similar results (Figure 9a), as well as $T_{SD,d}$ and $T_{Ra,d}$ (Figure 9c). $T_{min,d}$ had a different matrix comparison (Figure 9b) compared to the other statistics. The four years in each weather station had no significant differences (black blocks) except for $T_{min,d}$ at the *Tla* weather station in 2016 and 2017. $T_{ave,d}$ and $T_{max,d}$ were significantly different among the weather stations in all years. $T_{min,d}$ was significantly different at the *Tla* weather station compared to the other three weather stations. $T_{SD,d}$ and $T_{Ra,d}$ at *Tla* weather stations were not significantly different compared with the *Hua* and the *LMII* weather stations. Among the other weather stations, they were. The average and maximum air temperature comparison matrix had $(26/48)*100= 54.16\%$ of grey blocks significantly different, the minimum air temperature comparison matrix had $(16/48)*100= 33.3\%$ of grey blocks. The standard deviation and range comparison matrix had $(17/48)*100= 35.4\%$ of grey blocks.

3.2.3. Principal component analysis of daily air temperature statistics

The accumulated total variance of $T_{ave,d}$, $T_{max,d}$, $T_{min,d}$, $T_{SD,d}$,

and $T_{Ra,d}$, represented by the principal components are shown in Figure 10. The PCA showed that three components represented about 90% of the accumulated total variance of $T_{ave,d}$ and $T_{min,d}$ statistics, while four components did it for $T_{max,d}$, $T_{SD,d}$, and $T_{Ra,d}$. Components 1, 2, and 3 represented about 75%, 9%, and 5% of $T_{ave,d}$ and $T_{min,d}$ total variance, respectively. $T_{SD,d}$, and $T_{Ra,d}$ had a similar representation of accumulated variance by the components, the first three components represented 79% of the accumulated total variance. Components 1, 2, and 3 represented about 44%, 23%, and 12% of the accumulated total variance of $T_{SD,d}$, and $T_{Ra,d}$. $T_{max,d}$ was represented in less measure for the first three components with a value of 77%. Components 1, 2, and 3 represented 37%, 24%, and 16% of the accumulated total variance of $T_{max,d}$, respectively.

The correlations or L values (equation 4) of the sixteen weather station-year groups, with two principal components, are shown in Figure 11. It can see that the dots, which represent a weather station and a year of $T_{ave,d}$ and $T_{min,d}$ had similar dot distribution in the graph but different positions for each specific weather-year group (Figures 11a and 11c). $T_{SD,d}$ and $T_{Ra,d}$ had similar dots distribution and position (Figures 11d and 11e). The dots of $T_{max,d}$ (Figure 11b) differ concerning the other four statistics. The correlations between $T_{ave,d}$ and component 1 was around -0.78 to -0.92, and the correlations with component 2 were about -0.38 to 0.55 (red lines). $T_{ave,d}$ of four weather stations in 2016 formed a group because they had positive correlations of about 0.5 with component 2. The correlations between $T_{max,d}$ and component 1 was about -0.06 to -0.82, and the correlations with component 2 were about -0.37 to 0.93. The four weather stations in 2016 formed a group because their correlation rounded 0.9 with component 2. $T_{min,d}$ had correlations with component 1 from -0.91 to -0.79 and with component 2, from -0.91 to -0.79. $T_{min,d}$ in 2019 had the lowest correlation with component 2, while in the $T_{ave,d}$ analysis, the weather stations in 2017 had the lowest correlations with this component. $T_{SD,d}$ and $T_{Ra,d}$ had correlations of about -0.05 to -0.9 with component 1 and about -0.9 to 0.4 with component 2. Due to this, the weather stations of 2017, 2018, and 2019 formed a group, while the weather stations of 2016 formed another.

3.3 Monthly air temperature

The average, minimum, maximum, standard deviation, and monthly range of air temperature, calculated grouping T_{10} data by month are shown in Figure 12. The highest values of the monthly average ($T_{ave,m}$) and maximum ($T_{max,m}$) were observed from April to May, and the lowest in December and January. These parameters were the lowest in the north and south forest weather stations, followed by the agricultural and urban weather

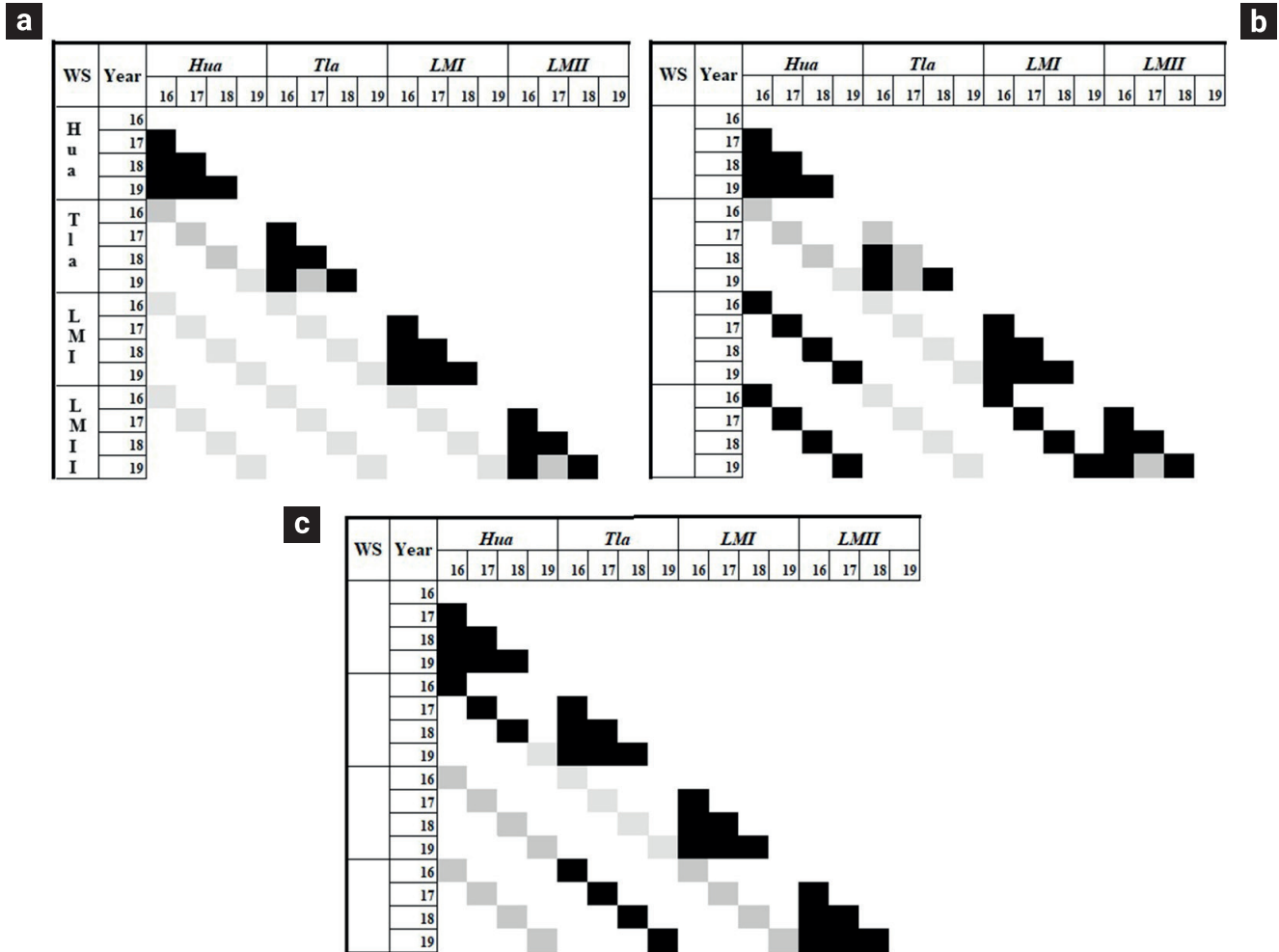


Figure 9. Comparison of daily air temperature statistics: a) average and maximum, b) minimum, c) standard deviation and range. Black box = no significant difference, grey box = significant difference. WS = Weather station.

Table 4. Statistics of minimum and maximum daily air temperature.

Weather station	n	Minimum daily air temperature					
		Ave	Min	Max	Kurtosis	Skewness	S. D.
Tla	1212	8.9	-2.8	15.4	-0.28	-0.60	3.33
Hua	1398	5.2	-9.4	13.6	-0.20	-0.40	4.15
LMI	1329	5.7	-1.4	11.9	-0.25	-0.45	2.34
LMII	1265	5.6	-3.5	12.0	-0.20	-0.42	2.84
Weather station	n	Maximum daily air temperature					
		Ave	Min	Max	Kurtosis	Skewness	S. D.
Tla	1212	25.4	10.7	32.7	1.97	-0.70	2.73
Hua	1398	22.8	8.5	30.0	1.44	-0.58	2.68
LMI	1329	18.8	7.2	28.1	0.16	-0.08	3.15
LMII	1265	21.2	8.3	32.9	1.46	-0.48	2.84

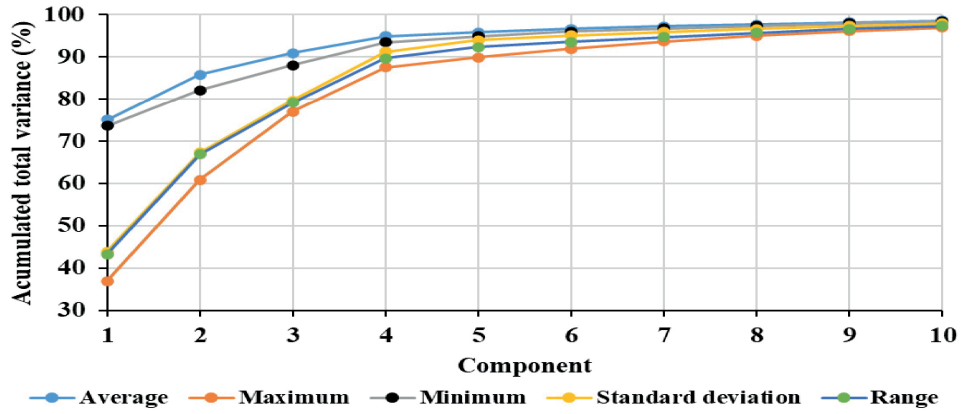


Figure 10. The accumulated total variance of principal components for daily air temperature statistics.

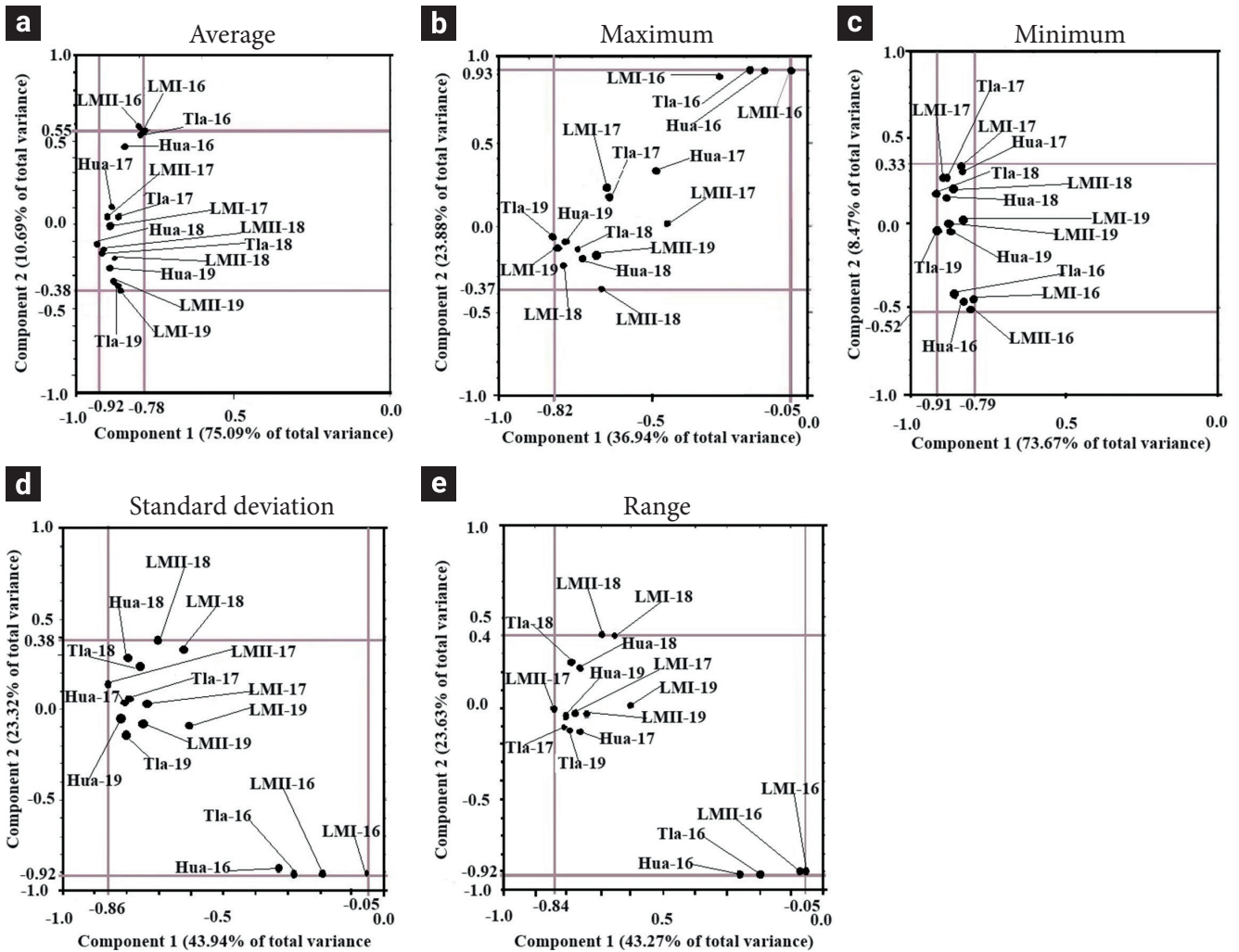


Figure 11. Daily air temperature statistics correlations with two principal components for weather stations-years groups.

stations. The lowest values of the monthly minimum ($T_{min,m}$) were in January, and the highest were from June to October. $T_{min,m}$ values were higher in the urban weather station and dropped in the agricultural weather station. The monthly standard deviation ($T_{SD,m}$) and range ($T_{Ra,m}$) presented upper values from November to January and lower ones from June to October. $T_{SD,m}$ and $T_{Ra,m}$ presented the lowest values in the north and south forest weather stations, and the highest values in the agricultural weather station.

Figure 12 shows that $T_{ave,m}$, $T_{max,m}$, and $T_{min,m}$ had an increasing stage from January to May, a flat line from June to July, and a decreasing stage from August to December. The $T_{SD,m}$ and $T_{Ra,m}$ behaviors were opposite to $T_{ave,m}$, $T_{max,m}$, and $T_{min,m}$. In the phases from January to May and from August to December, the inter-monthly changes of $T_{ave,m}$ and $T_{min,m}$ were more noticeable than $T_{max,m}$, $T_{SD,m}$ and $T_{Ra,m}$. In the January to May phase, $T_{ave,m}$, $T_{max,m}$ and $T_{min,m}$ showed positive and $T_{SD,m}$ and $T_{Ra,m}$ negative slopes, with values of 1.5, 1.2, 1.9, -0.2, and -0.8 °C/month, respectively. From August to December, the changes were the opposite, with negative slopes of $T_{ave,m}$, $T_{max,m}$ and $T_{min,m}$ and

positive for $T_{SD,m}$ and $T_{Ra,m}$, with values of -1.0, -0.2, -1.7, 0.47, and 1.5°C/month, respectively.

4. Discussion

4.1 Diurnal air temperature

4.1.1 warming and cooling rates

The statistics analyzed (average, minimum, maximum, and range) had different values between warming and cooling rates in the sixteen groups (Figure 5), except for standard deviation, which had values rounded to $1.0 \times 10^{-2} \text{ °C} \cdot 10 \text{ min}^{-1}$ in both types of rates. The average warming and cooling rates fluctuated similarly between groups, but with opposite sign rounding $3.0 \times 10^{-2} \text{ °C} \cdot 10 \text{ min}^{-1}$ for warming rates and $-3.0 \times 10^{-2} \text{ °C} \cdot 10 \text{ min}^{-1}$ for cooling rates. The minimum rates had more fluctuation between the groups in the cooling phase than in the warming

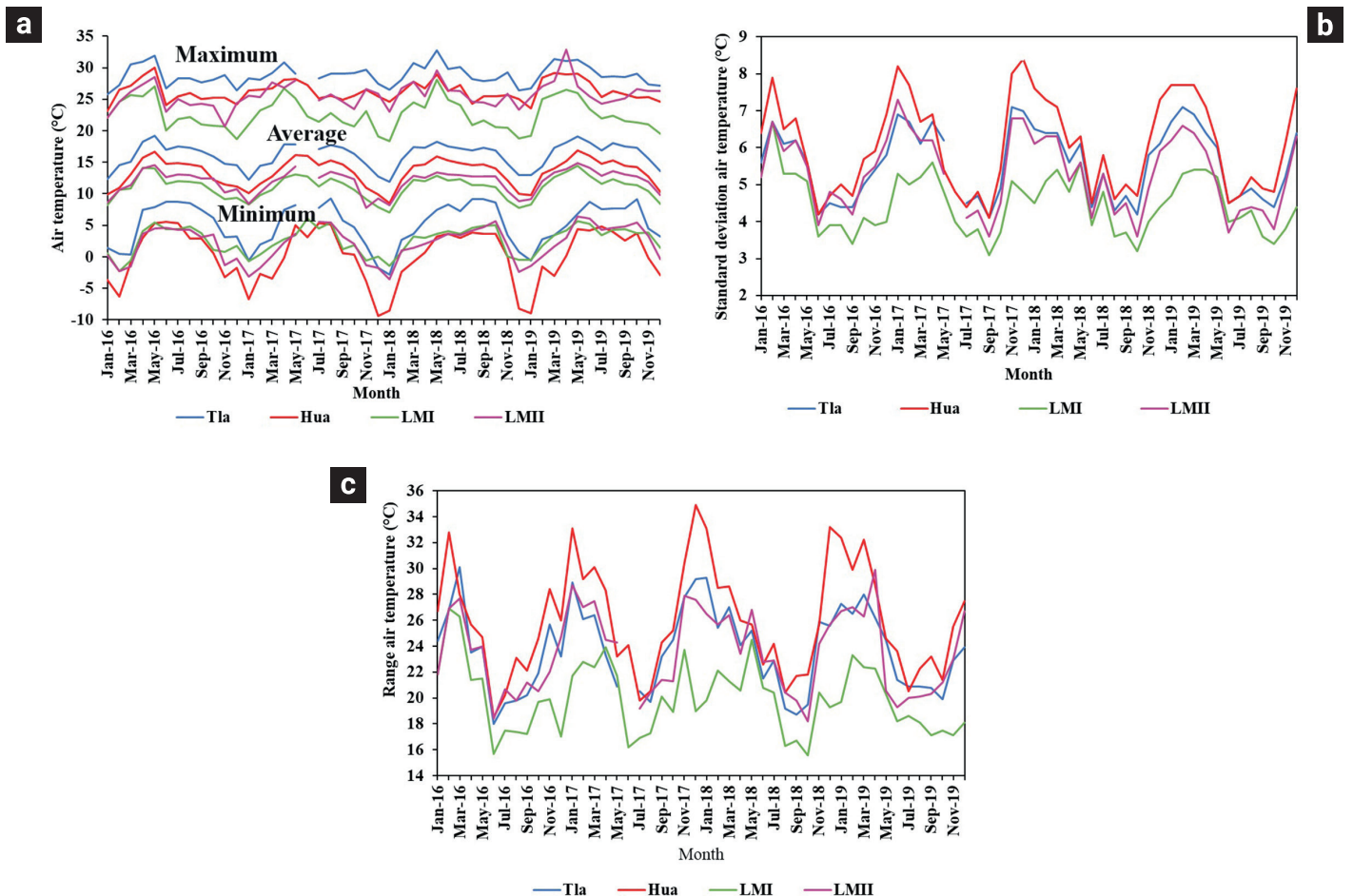


Figure 12. Monthly air temperature statistics: a) average, maximum, and minimum, b) standard deviation, c) range.

phase. The highest minimum values of cooling rates are in the forest (LMI weather station) and the lowest in urban (Tla weather station in 2016) and agriculture (Hua weather station in 2016), it may be because 2016 was an El Niño year (Martínez *et al.*, 2017). In contrast to the minimum, the maximum had more fluctuation in the warming phase than in the cooling phase. However, the lowest values of maximum warming rates are in forests and the highest in agriculture and urban weather stations. The range of warming rates was dissimilar to the range of cooling rates. These results show that the vegetation of the forests dampens the air warming by biophysical mechanisms (Li *et al.*, 2015) and by the suppression of mixing due to the lower roughness of the open areas, which causes the temperatures to rise more rapidly than in the forests (Lee *et al.*, 2011). However, these differences between the forest and the agricultural area can also be caused by elevation in sites (Good, 2015; Hemond and Fechner, 2015).

4.1.2 Comparing heating and cooling rates

Multiple comparisons of warming rates between the weather stations-years combinations, with the K-W test, and comparisons of cooling rates showed that environmental conditions heat up at similar rates in 87.5% of combinations and cool down in 73%. The consistent warming rates differences between agricultural (Hua weather station) and forest of the north side of La Malinche volcano (LMI weather station) in 2016, 2018, and 2019 stand out. The cooling rates significantly differed between the agricultural, urban, and forest areas of the north side of La Malinche volcano and between the north and south forests of La Malinche volcano (Figure 4b). The forest cooling rates of the north slope of La Malinche volcano (LMI weather station) are higher than the south forest (LMII weather station). The differential cooling rates in La Malinche volcano can be due to its symmetrical conical shape, its location in the north latitude, and that it is an isolated volcano in the trans-Mexican volcanic belt (Castro-Govea and Siebe, 2007), all of them causing that the north side is less exposed to the sun. Nevertheless, the cooling rate of the forest's south slope is comparable to the agricultural and urban areas.

4.1.3 Principal component analysis of warming and cooling rates

The PCA showed that three components represented the total variances of the warming and cooling rates, rounding 80%. This percentage was comparable to those reported in the analysis of other climatological variables (Bethere *et al.*, 2017; Isaak *et al.*, 2018; Zuška *et al.*, 2019). In general, this indicated that warming and cooling rates in the sixteen groups of weather stations-years meet the criteria that the groups can be a linear combination

(Schuenemeyer and Drew, 2011) or covariate similarly (Hurth and Pokorna, 2005). However, the variance values components indicate that air temperature warming rates were partially a linear combination forming two groups among years, one for 2017, 2018, and 2019 and another for 2016. This result indicates a perturbation relating air temperature among the urban, agricultural, and forest environments studied. Concerning cooling rates, the linear combination was weaker; in other words, there was more perturbation because the variance representativeness of component 1 was equal to 40%. In this case, the dots representing weather stations-year were more disperse, according to Figures 7a and 7b. The dots distribution in Figures 7a and 7b also indicates that the air temperature warming rates are different from cooling rates. This clearly shows the effect of forest, agriculture, and urbanization. If variation in air temperature were due to the altitudinal and spatial gradient, then the dots would be concentrated in some place on the graphic and would be a perfectly linear combination with rounding values of 100% by the first principal component. Consequently, the PCA could be a valuable tool to detect changes in air temperature gradient caused by perturbation of the system.

4.2 Daily air temperature

4.2.1 Average, minimum, maximum, standard deviation, and range

The analysis of air temperature statistics showed that the lines of the average and the maximum urban weather station were on top in the graphics, followed by agricultural, south forest, and north forest of La Malinche volcano. The minimum air temperature had behavior where the urban weather station was on top, followed by south forest, north forest, and agricultural weather stations. The standard deviation and range were similar to the average and the maximum, but agriculture had the highest values, followed by urban and forest weather stations. The average, maximum, standard deviation, and range in the forest were lower than in agricultural and urban areas. The average and maximum difference is due to altitude (Hemond and Fechner, 2015; Chen *et al.*, 2018; Isaak *et al.*, 2018), which between forest and urban and agricultural weather stations is from 500 to 700m (Table 1). However, the differences in daily temperature between urban and agricultural areas cannot be attributed to the effect of altitude since there is a difference of 10 meters between them. The lower values of standard deviation and range in the forest are possibly due to the vegetation cover. The literature describes that forests have an important but complex role in air temperature (Li *et al.*, 2015; Lee *et al.*, 2011; Shiflett *et al.*, 2017; De Frenne *et al.*, 2019). The minimum air temperature values in the forest were

between urban and agricultural, which means that the forest buffers air temperature.

The $T_{ave,d}$ and $T_{max,d}$ most frequent values were higher in the urban environment than in agricultural and forest. That could be because, in urban areas, the air temperature increases with its size compared to its surroundings (Zhuo *et al.*, 2017). The $T_{max,d} > 30^\circ\text{C}$ occurs when a heatwave is presented (Rosenzweig *et al.*, 2006). A heatwave was registered throughout the country in 2019, which caused the air temperature rise above 30°C (Pascual *et al.*, 2019) in the urban areas but not in forest and agricultural ones.

The $T_{min,d}$ most frequent values in the urban area were higher than in the agricultural and forest areas. In the agricultural area, devoid of vegetation in winter, the highest number of days with temperatures below 0°C , caused by cold fronts, were recorded (Pascual *et al.*, 2019). The urban area had fewer days, with $T_{min,d} < 0^\circ\text{C}$ and more days with $T_{max,d} > 30^\circ\text{C}$. In agricultural areas, there were more days with $T_{min,d} < 0^\circ\text{C}$, than in urban and forest areas. This result clearly shows that the forests buffer the ambient temperature because they did not show $T_{min,d} < 0^\circ\text{C}$ in the agricultural area nor $T_{max,d} > 30^\circ\text{C}$ in the urban area.

The most frequent values of $T_{SD,d}$ and $T_{Ra,d}$ in the agricultural area were higher than in urban and forest areas, accentuating the $T_{Ra,d}$ difference between the agricultural and forest areas because the vegetation cover reduces the range temperature (Lee *et al.*, 2011). In winter, $T_{Ra,d}$ was higher than in summer-autumn in the three environmental conditions; this result is comparable to that reported in the literature (Qu *et al.*, 2014). In winter, $T_{Ra,d}$ is higher due to the lack of cloudiness (Braganza *et al.*, 2004; Roy and Balling Jr., 2005), cold fronts (Pascual *et al.*, 2019), and the lack of vegetation cover (Lee *et al.*, 2011), which cause more significant fluctuations in temperature during the day.

4.2.2 Comparing daily air temperature statistics.

According to the environmental conditions analyzed, we expected that the air temperature differences could be among urban, agricultural, and forest, but not among years. Indeed, regarding the latter, the K-W test showed that among years, there were no significant differences, except for minimum air temperature at urban conditions. The K-W test showed that the environment conditions analyzed were significantly different ($p < 0.05$) based on $T_{ave,d}$ and $T_{max,d}$. With $T_{min,d}$, $T_{SD,d}$ and $T_{Ra,d}$, the differences between the environmental conditions were not consistent. It is plausible to say that the temperature differences between urban and agricultural areas are not due to altitude because both have a difference of 10 m, but according to their environmental conditions and the differences between the north forest and the south forest are due to position in the La Malinche volcano. The

north forest is located at a higher altitude and is less exposed to solar radiation compared to the south forest, which is located at a lower altitude and is more exposed to solar radiation.

4.2.3 Principal component analysis of daily air temperature statistics

The PCA showed that the total variances of $T_{ave,d}$ and $T_{min,d}$ were represented ($>80\%$) by two components, while $T_{max,d}$, $T_{SD,d}$ and $T_{Ra,d}$, by three components. Similarly to warming and cooling rates, the analysis using five statistics indicated that daily air temperature can be a linear combination (Schuenemeyer and Drew, 2011; Hurth and Pokorna, 2005) but with a perturbation degree characterized by the variance of components. The correlation values (Figure 10) showed that the linear combination of the environmental conditions is based on years. The statistics (T_{max} , and $T_{Ra,d}$) for 2016 resulted in a partially linear combination, and those for 2017, 2018, and 2019 resulted in another. This result reveals that although the thermal gradient is still preserved in the study area, if the urbanization and the agricultural regions continue increasing, and so does the reduction of the forest, the natural thermal gradient is at risk of breaking. The conjugation of the results of the K-W test and the PCA showed that the temperatures had significant differences and were a partially linear or perturbed combination.

4.3 Monthly air temperature

The monthly behavior of $T_{ave,m}$, $T_{max,m}$ and $T_{min,m}$ showed that the values were higher in April and May and lower in winter. This is probably due to the minimization of topographic factors during the winter months, the short duration of the day, and the lowest angle at which the sun's rays strike the earth's surface (Dutta *et al.*, 2017). In the agricultural area, the inter-monthly changes of $T_{ave,m}$, $T_{min,m}$, $T_{SD,m}$ and $T_{Ra,m}$, were more significant than in the forest and the urban area. This result is comparable to that reported in the literature (Shiflett *et al.*, 2017; Rushayati *et al.*, 2018; Wong and Peck, 2005). The inverse behavior of $T_{SD,m}$ and $T_{Ra,m}$ concerning $T_{ave,m}$, $T_{max,m}$ and $T_{min,m}$, shows the effect of rainfall and cold fronts in the study area from May to June and November to February, respectively.

The $T_{ave,m}$ in the agricultural and forest areas was lower than average monthly air temperature (1981-2010), while in the urban areas, they were higher in March, April, October, November, and December 2019. In these months, Pascual *et al.* (2019) reported similar monthly temperatures on a national scale (Mexico). Concerning the monthly $T_{max,m}$, they were lower than their respective normal ones in the three environmental conditions. There weren't significant differences between the

$T_{max,m}$ and normal ones in the agricultural area, while the most considerable difference was in the forest.

In the three environmental conditions, the monthly $T_{min,m}$ was higher than the average minimum air temperature. Monthly $T_{min,m}$ increasing was more accentuated in urban areas than in agriculture and forest areas. The $T_{min,m}$ increased more than the monthly $T_{max,m}$; this result is consistent with that reported in other studies (Qu *et al.*, 2014; Machiwal *et al.*, 2019). From January to May, the monthly changes of $T_{ave,m}$, $T_{max,m}$ and $T_{min,m}$ were lower than those reported by Chinchorkar *et al.* (2013), but the changes from August to December were more significant than those of the same authors. The monthly changes of $T_{min,m}$ were comparable to those reported in the literature (López-Díaz *et al.*, 2013; Colunga *et al.*, 2015).

5. Conclusions

The five statistics (average, minimum, maximum, standard deviation, and range) had no values persistent in warming and cooling rates. The K-W test showed that warming and cooling rates are significantly different between the agricultural, urban, and forest areas. Even the north and south sides of La Malinche volcano have a significant difference in cooling rate. The PCA showed that the warming and cooling rates were partially a linear combination in the agricultural, urban, and forest. Still, cooling rates had less value of variance, indicating a high degree of perturbation in these environmental conditions. In others words the cooling rate is more sensitive to show the system perturbation.

The average, maximum, and minimum air temperature in urban, standard deviation, and range in agriculture had the highest values in graphics. These differences between urban and agricultural environments cannot be attributable to altitude but to cover vegetation and topography

Comparing air temperature along years, there were no significant differences except for minimum air temperature in the urban environment. The average and maximum daily air temperatures significantly differed between the environmental conditions. The daily air temperature on the north side of La Malinche resulted in a significant difference concerning the south side, likely due to solar radiation incidence.

The maximum, standard deviation, and range daily air temperature in urban, agricultural, and forest environments showed more perturbation degrees than average and minimum air temperature. The statistics of air temperatures showed significant differences in the environments, and the PCA showed that they are perturbed.

The monthly behavior of average, maximum, and minimum air temperature showed that the values were higher in April and

May and lowered in winter; standard deviation and range had inverse behavior. The average monthly air temperature in the agricultural and forest areas was lower than the normal monthly air temperature (1981–2010). While in the urban area, they were higher in March, April, October, November, and December. The monthly minimum air temperature increase was more accentuated in urban areas than in agriculture and forest areas, and the minimum increased more than the maximum monthly.

6. References

- Abid A., Zhang M. J., Bagaria V. K., & Zou J. (2018). Exploring patterns enriched in a dataset with contrastive principal components. *Nature Communications*, 9(1), 1-7. doi: <https://doi.org/10.1038/s41467-018-04608-8>
- Ayandale A. (2017). Variations in urban surface temperature: an assessment of land use change impacts over Lagos metropolis. *Weather*, 72(10), 315-319. doi: <https://doi.org/10.1002/wea.3178>
- Bernhardt J., Carleton A. M., & LaMagna C. (2018). A comparison of daily temperature-averaging methods: spatial variability and recent change for the CONUS. *Journal of Climate (J. Clim.)*, 31, 979-996. doi: <https://doi.org/10.1175/JCLI-D-17-0089.1>
- Bethere L., Sennikovs J., & Batheres U. (2017). Climate indices for the Baltic states from principal component analysis. *Earth System Dynamics*, 8(4), 951-962. doi: <https://doi.org/10.5194/esd-8-951-2017>
- Bloomer C., & Rehm G. (2014). *Using Principal Component Analysis to find correlations and patterns at diamond light source* (pp 19-21). Proceedings of IPAC, Dresden, Germany.
- Braganza K, Karoly DJ, Arblaster. (2004). Diurnal temperature range as an index of global climate change during the twentieth century. *Geophysical Research Letters*, 31(13), L13217. doi: <https://doi.org/10.1029/2004GL019998>
- Castro-Govea R, Siebe C. (2007). Late Pleistocene–Holocene stratigraphy and radiocarbon dating of La Malinche volcano, Central Mexico. *Journal of Volcanology and Geothermal Research*, 162(1-2), 20-42. doi: <https://doi.org/10.1016/j.jvolgeores.2007.01.002>
- Chen BX, Sun YF, Zhang HB, Han ZH, Wang JS, Li YK, Yang XL. (2018). Temperature change along elevation and its effect on the alpine timberline tree growth in the southeast of the Tibetan Plateau. *Advances in Climate Change Research*, 9(3), 185-191. doi: <https://doi.org/10.1016/j.accr.2018.05.001>
- Chinchorkar SS, Vaidya VB, Vyas P. (2013). Monthly, seasonal and annual air temperature variability and trends- a case study to assess climate change on Anand (Gujarat State). *Spring*, 1(1), 20-25.
- Colunga ML, Cambrón-Sandoval VH, Suzán-Azpiri H, Guevara-Escobar A, Luna-Soria H. (2015). The role of urban vegetation in temperature and heat island effects in Querétaro City, Mexico. *Atmósfera*, 28(3), 205-218. doi: <https://doi.org/10.20937/ATM.2015.28.03.05>
- Daultrey S. (1976). *Principal components analysis: CATMOG Series*.

- Geo Abstracts Ltd.* University of East Anglia Norwich. <https://alex-singleton.files.wordpress.com/2014/09/8-principle-components-analysis.pdf>
- De Frenne P, Zellweger F, Rodríguez-Sánchez F, Scheffers BR, Hylander K, Luoto M, Vellend M, Verheyen K, Lenoir J. (2019). Global buffering of temperatures under forest canopies. *Nature Ecology and Evolution*, 3, 744-749. doi: <https://doi.org/10.1038/s41559-019-0842-1>
- Duffy KA, Schwalm CR, Arcus VL, Koch GW, Liang LL, Schipper LA. (2021). How close are we to the temperature tipping point of the terrestrial biosphere? *Science Advances*, 7(3), 1-8. doi: <https://doi.org/10.1126/sciadv.aay1052>
- Dutta PN, Karlo T, Dutta P. (2017). Some features of surface air temperature: a statistical viewpoint. *Environment and Ecology Research*, 5(5), 367-376. doi: <https://doi.org/10.13189/eer.2017.050506>
- Fernández EA, Romero CR, Zavala HJ. (2015). Redes de observación atmosférica y ambiental. Unidad de Informática para las Ciencias Atmosféricas y Ambientales (UNIATMOS). Red Universitaria de Observatorios Atmosféricos (RUOA). Centro de Ciencias de la Atmósfera, Universidad Nacional Autónoma de México. <https://atlasclimatico.unam.mx/acdm/visualizador>
- Fuelner G, Rahmstorf S, Leverman A, Volkwardt S. (2013). On the origin of the surface air temperature difference between the Hemispheres in Earth's present-day climate. *Journal of Climate*, 26(18), 7136-7150. doi: <https://doi.org/10.1175/JCLI-D-12-00636.1>
- García CF, Bestion E, Warfield R, Yvon-Durocher G. (2018). Changes in temperature alter the relationship between biodiversity and ecosystem functioning. *Proceedings of the National Academy of Sciences of the United States of America*. 115(43), 10989-10994. doi: <https://doi.org/10.1073/pnas.1805518115>
- Good E. (2015). Daily minimum and maximum surface air temperatures from geostationary satellite data. *Journal of Geophysical Research: Atmospheres*. *Journal of Geophysical Research: Atmospheres*, 120(6), 2306-2324. doi: <https://doi.org/10.1002/2014JD022438>
- Hajrya R, Mechbal N. (2013). Principal component analysis and perturbation theory-based robust damage detection of multifunctional aircraft structure. *Structural Health Monitoring*, 12(3), 263-277. doi: <https://doi.org/10.1177/1475921713481015>
- Hemond HF, Fechner EJ. (2015). The atmosphere. En Academic Press (Ed.), *Chemical fate and transport in the environment* (311-354 pp.). Academic Press.
- Hu Y, Mskey S, Uhlenbrook S. (2012). Trends in temperature and rainfall extremes in the Yellow River source region, China. *Climatic Change*. 110, 403-429. doi: <https://doi.org/10.1007/s10584-011-0056-2>
- Hurth R and Pokorna L. (2005). Simultaneous analysis of climatic trends in multiple variables: an example of application of multivariate statistical methods. *International Journal of Climatology* (. 25, 469-484. doi: <https://doi.org/10.1002/joc.1146>
- Intiaz H, and Sarwate AD. (2016). *Symmetric matrix perturbation for differentially-private principal component analysis*. [Presentación de paper]. International Conference on Acoustics, Speech and Signal Processing, Shanghai, China. doi: <https://doi.org/10.1109/ICASSP.2016.7472095>.
- Isaak DJ, Luce CH, Chandler GL, Horan DL, Wollrab SP. (2018). Principal components of thermal regimes in mountain river networks. *Hydrology and Earth System Sciences*, 22, 6225-6240. doi: <https://doi.org/10.5194/hess-22-6225-2018>
- Jolliffe IT, Cadima J. (2016). Principal components analysis: a review and recent developments. *Philosophical Transactions A*, 374(2065), 2-16. doi: <https://doi.org/10.1098/rsta.2015.0202>
- Lee X, Goulden ML, Hollinger DV, Barr A, Black TA, Bohrer G, et al. (2011). Observed increase in the local cooling effect of deforestation at higher latitudes. *Nature*, 479, 384-387. doi: <https://doi.org/10.1038/nature10588>
- Li D, Bou-Zeid E. (2013). Synergistic interactions between urban heat islands and heat waves: the impact in cities is larger than the sum of its parts. *Journal of Applied Meteorology and Climatology*, 52, 2051-2064. doi: <https://doi.org/10.1175/JAMC-D-13-02.1>
- Li Y, Zhao M, Motesharrei S, Mu Q, Kalnay E, Li S. (2015). Local cooling and warming effects of forest based on satellite observations. *Nature Communications*, 6, 6603. doi: <https://doi.org/10.1038/ncomms7603>
- López-Díaz F, Conde C, Sánchez O. (2013). Analysis of indices of extreme temperature events at Apizaco, Tlaxcala, Mexico: 1952-2003. *Atmósfera*. 26(3), 349-358.
- Machiwal D, Gupta A, Jha MK, Kamble T. (2019). Analysis of trend in temperature and rainfall time series of an Indian arid region: comparative evaluation of salient techniques. *Theoretical and Applied Climatology*, 136, 301-320. doi: <https://doi.org/10.1007/s00704-018-2487-4>
- Martínez R, Zambrano E, Nieto JJ, Costa F. (2017). Evolución, vulnerabilidad e impactos económicos y sociales de El Niño 2015-2016 en América Latina. *Investigaciones Geográficas*, 68, 65-78.
- McBean EA and Rovers FA. (1998). *Statistical procedures for analysis of environmental monitoring data and risk assessment*. New Jersey: Prentice Hall.
- Norma Mexicana: NMX-AA-166/1-SCFI-2013. (4 de septiembre 2013). Diario Oficial de la Federación, México. https://www.gob.mx/cms/uploads/attachment/file/166835/nmx-aa-166-1-scfi-2013_1_.pdf
- Nwofor OK, Dike VN. (2010). Daytime surface air temperature variations at locations in Owerri Capital City: indications of urban heat island build-up? *Advances in Science and Technology*, 4(2), 91-97. <https://advanscitech.com/nwofordike42.pdf>
- Oleson K. (2012). Contrasts between urban and rural climate in CCSM4 CMIP5 climate change scenarios. *Journal of Climate*, 25, 1390-1412. doi: <https://doi.org/10.1175/JCLI-D-11-00098.1>
- Pascual RR, López QM, Chablé PLA, Espejo MAZ, Loranca DY, Ledesma LJI, Quintero VEY. (2019). *Reporte del clima en México: Reporte anual 2019*. CONAGUA, México. <https://smn.conagua.gob.mx/es/reportes-del-clima-en-mexico>
- Pascual RR, López QM, Martínez SJN, Chablé PLA, Espejo MAZ,

- Ledezma LJI. (2018). *Reporte del clima en México: Reporte anual 2018*. CONAGUA, México. <https://smn.conagua.gob.mx/es/reportes-del-clima-en-mexico>
- Peterson TC. (2003). Assessment of urban versus rural in situ surface temperatures in the Contiguous United States: No difference found. *Journal of Climate*, 26(18), 2941-2959. doi: [https://doi.org/10.1175/1520-0442\(2003\)016<2941:AOUVRI>2.0.CO;2](https://doi.org/10.1175/1520-0442(2003)016<2941:AOUVRI>2.0.CO;2)
- Protsiv M, Ley C, Lankester J, Hastie T, Parsonnet J. (2020). Decreasing human body temperature in the United States since the Industrial Revolution. *eLIFE*, 9(e49555). doi: <https://doi.org/10.7554/eLife.49555>
- Qu M, Wan J, Hao X. (2014). Analysis of diurnal air temperature range in the continental United States. *Weather and Climate Extremes*, 4, 86-95. doi: <https://doi.org/10.1016/j.wace.2014.05.002>
- Radons SZ, Heldwein AB, Loose LH, Bortoluzzi MP, Brand SI, Engers LBO. (2019). Modeling hourly air temperature based on internationally agreed times and the daily minimum temperature. *Revista Brasileira de Engenharia Agrícola e Ambiental*, 23 (11), 807-811
- Rahman MA, Kang S, Nagabhatla N, Macnee R. (2017). Impacts of temperature and rainfall variations on rice productivity in major ecosystems of Bangladesh. *Agriculture and Food Security*, 6(10). doi: <https://doi.org/10.1186/s40066-017-0089-5>
- Rosenzweig C, Solecki W, Parshall L, Gaffin S, Lynn B, Goldberg R. et al. (2006). *Mitigating New York City's heat island with urban forestry, living roofs, and light surfaces*. 86th AMS Annual Meeting.
- Roy and Balling Jr. (2005). Analysis of trends in maximum and minimum temperature, diurnal temperature range, and cloud cover over India. *Geophysical Research Letters*, 32(12), L12702. doi: <https://doi.org/10.1029/2004GL022201>
- Ruíz AO, Espejel TD, Ontiveros CRE, Enciso JM, Galindo RMA, Quesada PML et al. (2016). Monthly trend of maximum and minimum temperatures in Aguascalientes, Mexico. *Revista Mexicana de Ciencias Agrícolas*, 13, 2535-2549.
- Rushayati SB, Shamila AD, Prasetyo. (2018). The role of vegetation in controlling air temperature resulting from urban heat island. *Forum Geografi*, 32(1), 1-11. doi: <https://doi.org/10.23917/forgeo.v32i1.5289>
- Schuenemeyer JH, Drew LJ. (2011). *Statistics for earth and environmental scientists*. New Jersey: John Wiley and Sons. <https://www.wiley.com/en-us/Statistics+for+Earth+and+Environmental+Scientists-p-9780470584699>
- Shiflett SA, Liang LL, Crum SM, Feyisa GL, Wang J, Janerette GD. (2017). Variation in the urban vegetation, surface temperature, air temperature nexus. *Science of the Total Environment*, 579, 495-505. doi: <https://doi.org/10.1016/j.scitotenv.2016.11.069>
- Sun L. (2016). Distribution of the temperature field in a pavement structure. L. Sun (Ed.). In: *Structural behavior of asphalt pavements* (pp. 61-177). Butterworth-Heinemann. doi: <https://doi.org/10.1016/B978-0-12-849908-5.00002-X>.
- Suomi J, Käyhkö J. (2012). The impact of environmental factors on urban temperature variability in the coastal city of Turku, SW Finland. *International Journal of Climatology*, 32(3): 451-463. doi: <https://doi.org/10.1002/joc.2277>
- Vitt R, Gulyás Á, Matzarakis A. (2015). Temporal differences or urban-rural human biometeorological factors for planning and tourism in Szeged, Hungary. *Advances in Meteorology*, 25, 987576. doi: <https://doi.org/10.1155/2015/987576>
- Vuckovic M, Kiesel K, Mahdavi A. (2017). The extent and implications of the microclimatic conditions in the urban environment: a Vienna case study. *Sustainability*, 9, 177. doi: <https://doi.org/10.3390/su9020177>
- Waldock C, Dornelas M, Bates AE. (2018). Temperature-driven biodiversity change: disentangling space and time. *BioScience*, 68(11), 873-884. doi: <https://doi.org/10.1093/biosci/biy096>
- Wiesner S, Eschenbach A, Ament F. (2014). Urban air temperature anomalies and their relation to soil moisture observed in the city of Hamburg. *Meteorologische Zeitschrift*, 23(2), 143-157. doi: <https://doi.org/10.1127/0941-2948/2014/0571>
- Wong N. H., & Peck T.T. (2005). The impact of vegetation on the environmental conditions of housing estates in Singapore. *International Journal on Architectural Science*, 6(1), 31-37. https://www.bse.polyu.edu.hk/researchCentre/Fire_Engineering/summary_of_output/journal/journal_AS.html
- Yang Q., Huang X., & Li J. (2017). Assessing the relationship between surface urban heat islands and landscape patterns across climatic zones in China. *Scientific Report*, 7, 9337. doi: <https://doi.org/10.1038/s41598-017-09628-w>
- Zelenáková M., Purcz P., Hlavatá H., & Blišťan. (2015). Climate change in urban versus rural areas. *Procedia Engineering*, 119, 1171-1180. doi: <https://doi.org/10.1016/j.proeng.2015.08.968>
- Zhuo B., Rybski D., & Kropp J. P. (2017). The role of city size and urban form in the surface urban heat island. *Scientific Reports*, 7, 4791. doi: <https://doi.org/10.1038/s41598-017-04242-2>
- Zuška Z., Kopcińska J., Dacewicz E., Skowera B., Wojkowski J., & Ziernicka-Wojtaszek A. (2019). Application of the principal components analysis (PCA) method to assess the impact of meteorological elements on concentrations of particulate matter (PM10): A case study on the Mountain Valley (the Sącz Basin, Poland). *Sustainability*, 11, 6740. doi: <https://doi.org/10.3390/su11236740>